ADVANCED MATERIALS
www.advmat.de

Donor–Acceptor–Donor Triads with Flexible Spacers: Deciphering Complex Photophysics for Targeted Materials Design

Siyang Feng, Liangxuan Wang, Begoña Milián-Medina, Alfred J. Meixner, Min Sang Kwon, Soo Young Park, Reinhold Wannemacher, and Johannes Gierschner**

The complex photokinetics of donor–acceptor–donor triads with varying flexible spacer lengths (n = 4–10 carbon atoms) are investigated in liquid and solid solution, as well as in crystals, by steady-state and transient fluorescence spectroscopy combined with computational studies. For the short spacer (n = 4) in a liquid solution, dynamic charge-transfer (CT) state formation with subsequent, efficient exciplex emission is observed, effectively competing with quenching through electron transfer (eT) via a radical ion pair. In a solid solution, a fluorescent CT static complex is formed upon freezing for all spacer lengths. This allows the observations of a former seminal report on stimuli-responsive high-contrast fluorescence on/off switching in films of the triads to be reassigned (Adv. Mater. 2012, 24, 5487), now providing a holistic picture on varying spacer length. In fact, external stimuli of the film by modulating the geometry of the CT complex, which results in on/off fluorescence switching (for $n > 4$) or in a change of the emission color (n = 4). The work thus demonstrates how in-depth analysis of complex photophysics can be put to practical use in materials science.

1. Introduction

All-organic π-conjugated materials have found immense interest for applications in energy or materials conversion and sensing, for instance in organic solar cells (OSCs), light emitting diodes (OLEDs), field effect transistors (OFETs), sensors, or photocatalysts (OPCs). In the quest for novel, tailor-made materials, molecules with complex photophysical deactivation pathways are progressively explored, such as room temperature phosphorescence (RTP),[1] thermally activated delayed fluorescence (TADF),[2] non-Kasha emission,[3,4] dual emission (DE),[4,5] or exciplex formation.[6] In many of these processes, the generation, spectroscopic signatures, and subsequent deactivation of energetically low-lying charge transfer (CT) states, formed between electron donor (D) and acceptor (A) moieties, is of central importance. This is in particular evident for DA interfaces in OSCs,[7] for alternating DA structures in low-bandgap polymers in OSCs and OFETs,[8] luminescent mixed-stacked co-crystals,[9,10] TADF materials used in OLEDs[2,11,12] or as OPCs.[13,14] as well as for fluorescence switching in stimuli-responsive materials.[15,16,17] The generated CT states and their deactivation are a matter of ongoing discussions, as very significant dependencies are observed on the electronic properties of the D and A moieties, covalent versus noncovalent D–A linkage, and exact D–A positioning, as well as periodicity and dimensionality of the D/A arrangement. Therefore, a detailed understanding of the

S. Feng, L. Wang, R. Wannemacher, J. Gierschner
Madrid Institute for Advanced Studies
IMDEA Nanoscience
Calle Faraday 9
Ciudad Universitaria de Cantoblanco
Madrid 28049, Spain
E-mail: reinhold.wannemacher@imdea.org;
johannes.gierschner@imdea.org
L. Wang, A. J. Meixner, J. Gierschner
Institute of Physical and Theoretical Chemistry
Eberhard Karls University Tübingen
Auf der Morgenstelle 18, 72076 Tübingen, Germany
B. Milián-Medina
Department for Physical Chemistry
Faculty of Chemistry
University of Valencia
Avenida Dr. Moliner 50 Burjassot, Valencia 46100, Spain
M. S. Kwon
Department of Materials Science and Engineering
Seoul National University
Seoul 08826, Republic of Korea
S. Y. Park
Research Institute of Advanced Materials
Seoul National University
Seoul 08826, Republic of Korea

The ORCID identification number(s) for the author(s) of this article can be found under https://doi.org/10.1002/adma.202306678

DOI: 10.1002/adma.202306678

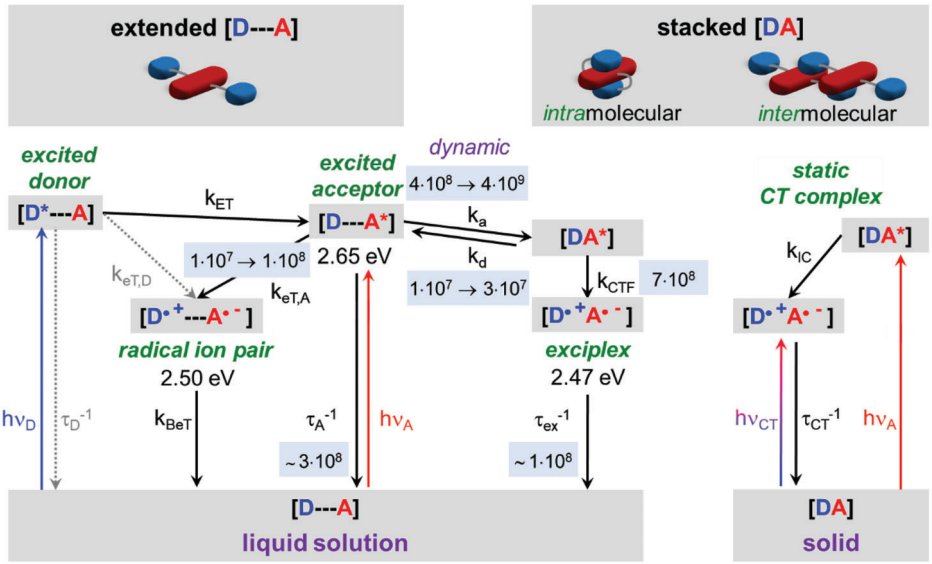

Scheme 1. Deactivation scheme of the D–σ–A–σ–D triads **DAD*n*** (n = 4–10) within the singlet state manifold under direct excitation of D or A for extended [$D^{\bullet+}A^{\bullet-}$], which prevails in liquid solution over stacked [DA]. Under D excitation, A^* is instantaneously formed by resonant energy transfer (ET), which here outcompetes electron transfer (eT_D). From A^*, sequential electron transfer (eT_A) to form the radical ion pair [$D^{\bullet+}\cdots A^{\bullet-}$], and subsequent quenching by back electron transfer (BeT) and vibrational relaxation, competes with A^* deactivation τ_A^{-1} (via fluorescence and IC). Alternatively, an exciplex [$D^{\bullet+}A^{\bullet-}$] is formed via a pre-associated complex [DA^*] with an association constant k_a, where the excitation is still localized on A, and which can re-dissociate with k_d; from here, subsequent CT formation (k_{CTF}) and exciplex deactivation through τ_{ex}^{-1} (via fluorescence and IC) occurs. Energies of relevant states (in eV) are obtained from single point TD-DFT (PBE0). Orders of rate constants are given (light blue shaded numbers, in s^{-1}); indicating the evolution (→) from n = 4 to 10, as resulting from photokinetic fitting (see Section 2: Results and Discussions). On the right, photoexcitation—and deactivation of the stacked [DA] CT complex is shown, which is formed in solid solution or molecular solids in the ground state, either in an intra- or intermolecular fashion.

underlying photophysics is of paramount interest for targeted materials design.

From a mechanistic understanding, the actual D–A distance within a pair (denoted as [DA] in **Scheme 1**) is particularly important, as only at short distances the low-lying CT singlet state (S_1) can be effectively populated upon direct or indirect photoexcitation via the singlet state manifold. Such close D–A separations can be realized in an *intra*molecular fashion by direct covalent D–A linkage[11,18] (including multiresonant structures[19]), or by short conjugated or non-conjugated spacers (i.e., D–π–A,[20] versus D–σ–A dyads[18,21]), as well as in an *inter*molecular noncovalent fashion through D:A complexes. The generated CT state can be emissive (i.e., with pronounced fluorescence quantum yield Φ_F), if the radiative rate k_r can successfully compete with the nonradiative rate k_{nr} (the latter typically proceeds via internal conversion; IC, with subsequent vibrational relaxation, VR) or intersystem crossing (ISC) to the triplet manifold. The radiative rate k_r scales with the oscillator strength f_{CT},[10,22] which depends on the overlap of the constituting molecular orbitals (MOs; or, in the possibly multiconfigurational description of the CT state, natural transition orbitals; NTOs) of D and A. This correlation with f_{CT} can be intuitively understood in a simple one-electron picture. In this framework, the CT character will be strong and f_{CT} therefore will be vanishing, if the highest occupied MO (HOMO) is localized entirely in D, and the lowest unoccupied MO (LUMO) is localized in A; otherwise partial CT, i.e., pCT, is observed with notable (or even rather large) f_{pCT}, as, e.g., in push–pull systems of organic chromophores (D–π–A).[20] The localization is mainly driven by the energetic offset of the MOs in the isolated D and A moieties,[18,23] but also by MO symmetry,[23] as well as connector type and position (e.g., meta versus para);[18,24] Importantly, also geometrical factors—in particular the twist angle between D and A—decides on the amount of CT;[2] such geometry change can also proceed dynamically during the excited state lifetime, as in compounds with twisted intramolecular CT (TICT) states.[25] For certain D–A systems with very pronounced CT character of the S_1–S_0 transition, ISC to the triplet manifold and subsequent reverse ISC from T_1 (due to the small exchange energy for the CT state) may give rise to TADF.[2,11]

If the separation between the D and A moieties is too large, a CT state cannot be directly photoexcited. Instead, the CT state may be dynamically generated after photoexcitation of D or A, see Scheme 1. This is commonly termed as an exciplex,[26,27] which may be created in mixed solutions of D and A molecules if the concentration is high enough to allow for the formation of an encounter complex, i.e., [$D^*\cdots A$] or [$D\cdots A^*$], during the lifetime τ of S_1; for this reason, pyrene is often utilized for excimer or exciplex formation, due to pyrene's very long τ.[28] Exciplexes can also be formed in molecular D–σ–A dyads with a flexible spacer s (i.e., independent of the concentration);[29,30] the relatively close separation also allows to use of chromophores with τ in the low nanosecond range.[27,29,31–33] Effective exciplex formation commonly requires short spacers,[32] in accordance with the "Hirayama" rule for excimers.[34] It should be noted in this context, that the exciplex term is now often used for noncovalent D:A complexes in the solid state, e.g. for TADF materials in OLEDs;[6] strictly speaking, these species are not "classic"

exciplexes, but rather intermolecular CT complexes, which, due to spatial confinement in the films, also exist in the ground state (see Scheme 1).

The specific signature of the exciplex is a bathochromically shifted, unstructured fluorescence with a prolonged lifetime; however, in most cases, exciplexes exhibit small Φ_F in solution, due to a combination of small k_r and high k_{nr}. In particular, for application in optoelectronics (OLEDs and sensors), it is therefore important to identify emissive dyads. The most important competitive path to exciplex formation after photoexcitation of D or A is photoinduced electron transfer (eT) to create a radical ion pair $[D^{\bullet+}\cdots A^{\bullet-}]$,[35] which is subsequently deactivated via back electron transfer (BeT) to the ground state (Scheme 1) or ISC.[35,36] In the context of exciplexes, this process was mainly investigated for initial photoexcitation of A,[27,29–32] where exciplex formation prevails in nonpolar environments, while eT dominates in polar solvents.[35] For excitation of D, on the other hand, photoinduced eT_D was intensively investigated as a competitive pathway to resonant energy transfer (ET; see Scheme 1) in molecular dyads with conjugated spacers (molecular wires);[37,38] these are in particular interesting as model systems for photosynthesis and organic electronics. In this context, $[D^{\bullet+}\cdots A^{\bullet-}]$, generated by eT, is commonly termed as "charge-separated" (CS) state,[37] in distinction to the CT state discussed above. The rate k_{eT} is usually thermally activated, as described, for instance, by the Marcus equation,[37,39] and was shown to exhibit an exponential spacer length dependence, expressed by the attenuation factor β_{eT}.[37] The latter depends on the electronic nature of D and A, as well as those of the linker, in particular on whether the linker consists of saturated hydrocarbons or conjugated strands, as well as on its specific geometry.

From the mentioned applications of molecular dyads and triads in optoelectronics, a seminal work by Kwon et al reported on D–σ–A–σ–D triads, based on a highly fluorescent *p*-distyrylbenzene-type A moiety, flexible, saturated hydrocarbon spacers of different chain length, and carbazole D moieties.[15] Significantly, films of these triads were shown to exhibit high contrast fluorescence on/off switching under external stimuli (temperature and pressure). Based on time-dependent density functional theory (TD-DFT) calculations, this was attributed back then to the occurrence of stacked/extended conformations of the triad. However, the exact mechanism was not further pursued at this point. In the current work, we thus decided to tackle this challenge by an in-depth investigation of these triads in solution, and under variation of polarity, viscosity, and temperature. Combining (steady-state and time-resolved) optical spectroscopy with computational studies (TD-DFT, and molecular dynamics, MD, simulations), we decipher herein the complex photophysical deactivation pathways of the triads, with respect to eT, dynamic exciplex formation, and the generation of a static CT complex upon spatial confinement of the triads. Technologically relevant is our identification of an optimized system, which shows red exciplex emission with a considerable Φ_F of 14%. Furthermore, our results evidence a new scenario for the stimuli-responsive behavior in the films, which rationalizes also the different behavior with varying spacer length; this may inspire further work in stimuli-responsive materials as well as in exciplex-based OLED, relying on the subtle interplay of complex photophysical deactivation pathways.

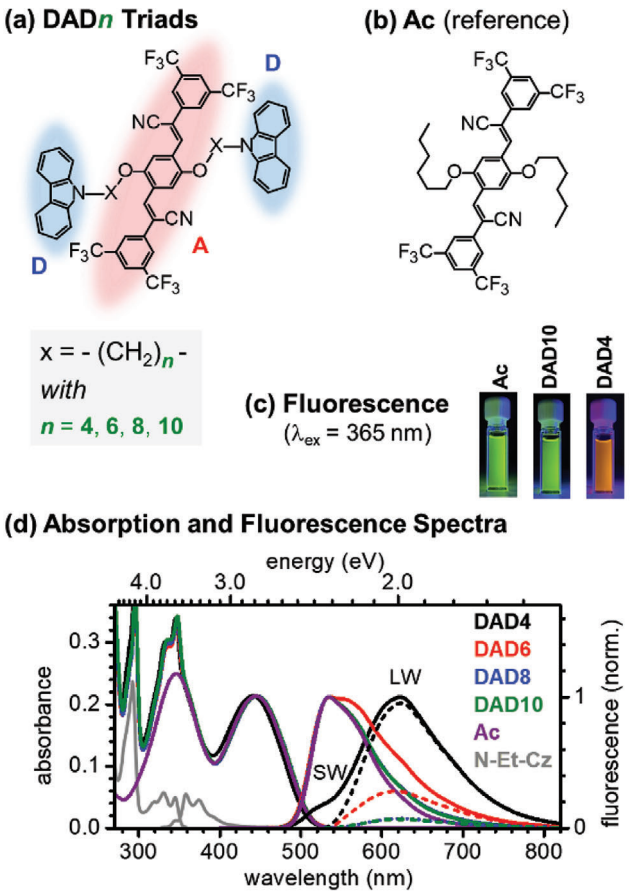

Figure 1. a,b) Molecular structures of the **DAD*n*** triads (a) and of reference **Ac** (b); c) fluorescence images of $CHCl_3$ solution; d) absorption (left) and fluorescence spectra (right) of the compounds in 10 μM $CHCl_3$ solution (**DAD8** fluorescence is superimposed by **DAD10**, being almost identical). The dashed lines are the long-wavelength components, obtained by spectral decomposition. Absorption and fluorescence spectra of the donor *N*-ethyl-carbazole (**N-Et-Cz**) are shown for comparison.

2. Results and Discussion

The investigated **DAD*n*** triads consist of a luminescent dicyano-substituted *p*-distyrylbenzene (DCS) acceptor (A) core with four CF_3 groups in the *meta*-positions, to which two carbazole donor (D) moieties are covalently attached via alkoxy linkers of different chain length (with n = 2, 4, 6, 8, 10 carbon atoms) at the central ring of the DCS core, see **Figure 1**. The reference acceptor molecule (**Ac**, see Figure 1) owns the same structure as the acceptor moiety of the triads, but carries hexyloxy-groups at the central ring. The cyano-groups of the acceptor are located in the outer positions of the vinylene-unit. Such *β*-substitution commonly generates highly fluorescent molecules, in particular in the presence of alkoxy-substituents, while IC and ISC are rather minor pathways.[40] It is reminded, that, on the contrary, DCS with *α*-substitution (in the inner vinylene position) are only very weakly luminescent due to efficient access to a conical intersection (CI);[40,41,42] in solid environments, solid-state luminescence enhancement (SLE) is then observed.[10,40]

Table 1. Spectroscopic data of the compounds in $CHCl_3$ solution at room temperature at short and long wavelength emission (SW, LW) with their corresponding emission maxima λ_{max}. Individual lifetimes (amplitudes) τ_i (A_i) are results of multiexponential fits, obtained at λ_{det} = 536 nm, 680 nm for SW and LW, respectively; τ_{PF} is the mean (intensity-weighted average) prompt lifetime (i.e., of the short components $\tau_{1,2}$), τ_{DF} is the delayed lifetime component, I_{DF} the respective fractional intensity, $\Phi_{F,tot}$ is the total fluorescence quantum yield, $\Phi_{F,i}$ are the quantum yields of the SW and LW components, obtained by spectral decomposition of the steady-state data in Figure 1 via the fractional intensities $x_{SW,LW}$.

		τ_1 (ns)[a]	A_1	τ_2 (ns)[a]	A_2	τ_{PF} (ns)[b]	τ_{rise} [ns]	A_{rise}	τ_{DF} [ns]	$A_{,DF}$	I_{DF}[c]	$\Phi_{F,tot}$	$\Phi_{F,i}$	λ_{max} (nm)
Ac	SW	0.87	0.12	3.47	0.88	3.39						0.41		535
DAD10	SW	0.64	0.20	1.47	0.80	1.39			8.56	0.009	0.054	0.30	0.27	535
	LW	0.33	0.13	1.30	0.87	1.27	–[d]		8.29	0.23			0.03	623
DAD8	SW	0.46	0.21	1.07	0.79	1.01			7.95	0.012	0.092	0.23	0.21	535
	LW	0.19	0.25	0.98	0.75	0.93	–[d]		7.68	0.18			0.02	615
DAD6	SW[e]	0.17	0.54	0.58	0.46	0.47			9.63	0.008	0.140	0.11	0.08	535
	LW	0.38	1.00	–	–	0.38	2.64	−0.21	9.51	0.25			0.03	620
DAD4	SW[f]	0.07	0.99	1.17	0.01	0.21			9.28	0.003	0.26	0.16	0.02	535
	LW						1.50	−1.01	9.92	1.00			0.14	620

[a] The accuracy is limited by the IRF (ca. 50 ps); [b] Intensity-weighted averaged lifetime; $\tau_{PF} = (A_1\tau_1^2 + A_2\tau_2^2)/(A_1\tau_1 + A_2\tau_2)$. Differences in τ_{PF} for SW and LW detection are within the experimental error of the setup; [c] $I_{DF} = A_{DF}\tau_{DF}/(A_1\tau_1 + A_2\tau_2 + A_{DF}\tau_{DF})$; [d] Contribution too small to be detected; [e] λ_{det} = 505 nm; [f] λ_{det} = 524 nm.

2.1. Optical and Photophysical Properties

The absorption spectrum of **Ac** shows unstructured "double hump" features with maxima at 347 nm and 445 nm, respectively (Figure 1). This arises from excited state splitting of the DCS core due to the presence of the alkoxy functionalities in the central ring;[40,43] The resulting states ($S_{1,2}$) are well described by one-electron excitations between the delocalized HOMO and HOMO-1, respectively, to the LUMO.[40] The fluorescence spectrum in non-polar solvents (e.g., *n*-octane) is vibronically structured (vide infra); in the more polar solvent $CHCl_3$ it appears unstructured and somewhat bathochromically shifted (to 535 nm, see Figure 1), due to minor (but not insignificant) CT contributions in the emitting state (S_1), as discussed below. In accordance with the previous findings on β-DCS compounds,[40,41] **Ac** is brightly fluorescent, emitting in $CHCl_3$ solution with a fluorescence quantum yield of Φ_F = 0.41, see **Table 1**; in non-polar solvents (*n*-octane, toluene) Φ_F rises to 0.60. The high Φ_F of **Ac** is correlated to the low Franck–Condon energy (2.79 eV; 445 nm), which successfully inhibits access to the CI.[40,41] The fluorescence decay of **Ac** in $CHCl_3$ (**Figure 2**) is nonexponential with a mean lifetime of 3.4 ns (in Table 1 denoted as prompt lifetime τ_{PF} in distinction from the delayed lifetime τ_{DF} observed for the exciplexes of the triads, vide infra). The non-exponential character of τ_{PF} pointing to significant geometry changes for **Ac** in the excited state (vide infra).

The absorption spectra of the **DAD*n*** triads in $CHCl_3$ solution are a simple superposition of those of the donor (carbazole) and acceptor (**Ac**) molecules alone,[15] see Figure 1. Only for **DAD4**, a small hypsochromic shift of the low energy absorption band is observed. In particular, for none of the triads, any indication for additional absorption by a CT state is found. The fluorescence excitation spectra of all triads follow closely the absorption spectra at all detection wavelengths (see Figure S8, Supporting Information). This is a direct proof[44] that there are no major additional loss channels after photoexcitation of D→D* (in particular by fluorescence of D*, or by photoinduced eT_D[37]); instead, A* is instantaneously prepared from D* by resonant (Coulomb-type) energy transfer (ET, through $D^* + A \rightarrow D + A^*$), that means in equal manner as under direct photoexcitation of A, see Scheme 1.

Different from absorption, the fluorescence properties vary strongly among the triads. The fluorescence spectra of **DAD10** and **DAD8** are very similar to that of **Ac**, but show a slight broadening on the low-energy side (vide infra). At the same time, the prompt lifetime τ_{PF} is reduced strongly and monotonically with *n* versus **Ac**, particularly in polar solvents (see Table 1, and Table S6 in the Supporting Information). At the same time, Φ_F is also reduced compared to **Ac**, although not as much as τ_{PF} (vide infra).

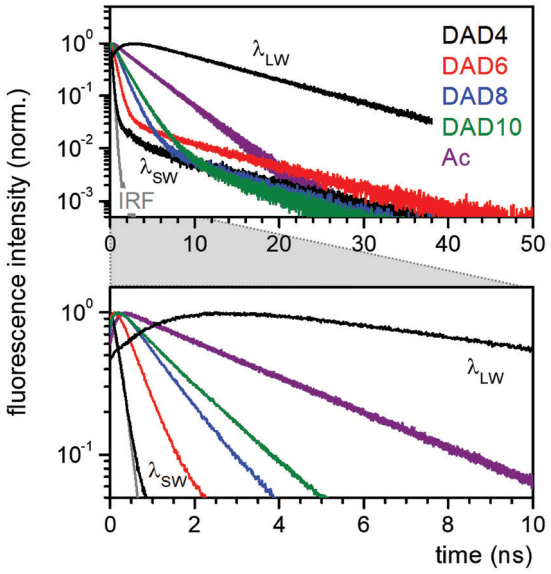

Figure 2. Fluorescence time traces of **Ac** and the **DAD*n*** triads in $CHCl_3$, detected at λ_{SW} = 536 nm (for *n* = 4, detection at λ_{SW} = 524 nm, λ_{LW} = 680 nm; for details see the Supporting Information) (top) and zoom into the time range up to 10 ns (bottom). The instrumental response function (IRF) is given as a gray line; details of the lifetime evaluations are given in Figure S10, Supporting Information.

One scenario for the emission quenching is eT (see Scheme 1), as commonly observed for D–σ–A dyads.[37] The different dependencies found for Φ_F and τ_{PF} as well as the time evolution of the emission features (vide infra), however, point to more complex photophysics.

This becomes in particular obvious for DAD4. In stark contrast to the triads with the long spacers, **DAD4** shows only a shoulder at short wavelengths (SW, Figure 1) in $CHCl_3$ solution, corresponding to the spectral position of **Ac**, with a short lifetime (≈0.2 ns), and a small fractional quantum yield of $\Phi_{F,SW} = 0.02$, see Table 1. Instead, a new emission appears at long wavelengths (LW), centered at $\lambda_{LW,max} = 623$ nm, which dominates the spectrum ($\Phi_{F,LW} = 0.14$). **DAD4** thus clearly exhibits dual emission.[4] Accordingly, the emission color changes from green (**Ac**, **DAD8**,**10**) to orange (**DAD4**), see Figure 1. The fluorescence excitation spectra of **DAD4**, recorded at λ_{LW} and λ_{SW}, are identical (Figure S8, Supporting Information), demonstrating that the population of the LW state is independent of excitation; thus, SW and LW emission originate from the same absorbing species. In particular, no direct photoexcitation of a CT state is observed in the excitation spectrum recorded at λ_{LW}. Furthermore, no concentration dependence was found upon dilution (see Figure S12, Supporting Information); this in all points to an intramolecular exciplex between the D and A moieties as the source of the LW emission, i.e., a CT state which is only dynamically formed by folding of the spacer during the excited-state lifetime. This agrees with the observed broad features of the LW emission, as typically found for exciplexes.[29–32] The dynamic nature of the exciplex formation is further confirmed by a fluorescence rise time of 1.5 ns in the transient fluorescence recorded at λ_{LW} (Table 1); the associated (delayed) decay time is long (τ_{DF} = 9.9 ns) and exhibits the same amplitude, indicative of a consecutive reaction. The long decay evidences also a small oscillator strength of the emitting state, being consistent with a pronounced CT character of the exciplex. We note that the rise time of exciplex emission does not correspond to the decay time of the SW emission; this compels the introduction of an intermediary step in the photokinetics, vide infra, Significantly, a long lifetime component is equally found under detection at 524 nm (Table 1) and even at 505 nm detection, but only as a minor component. As the corresponding energy is higher than the spectral onset of the exciplex emission extracted from spectral decomposition (see Figure 1, and Figure S9, Supporting Information), this points again to more complex photokinetics, vide infra. Finally, **DAD6** corresponds to an intermediate situation regarding the observed fluorescence in $CHCl_3$ (Figure 1), with significant broadening due to exciplex formation ($\lambda_{LW,max} = 616$ nm), being visible in the fractional $\Phi_{F,LW}$ as well as in the noticeable presence of the exciplex decay time τ_{DF}, see Table 1. The long decay component τ_{DF} can also be detected for long spacer length (**DAD8**, **DAD10**) in $CHCl_3$ when recorded at λ_{LW} (being somewhat shortened compared to **DAD4**, see Table 1); also here τ_{DF} is seen at λ_{SW}, but as a very minor component (Table 1). Spectral decomposition of the fluorescence spectra gives very similar exciplex feature as for **DAD4** with $\lambda_{LW,max} = 619$ nm, but as a contribution with much lower intensity, see Figure 1.

The increasing significance of exciplex formation with decreasing spacer length *n* can be specifically visualized by time-resolved emission spectra (TRES, recorded in $CHCl_3$). As shown in **Figure 3**; the SW emission appears for **Ac** and all **DAD*n*** triads at $t = 0$ with a constant spectral position of 533 nm; only for **DAD4**, a hypsochromic shift to 530 nm is observed, in accordance with the shift of the absorption band (vide supra). The decay of the SW emission becomes increasingly faster with decreasing *n*. Subsequently, the LW emission rises and slowly decays. However, the contribution of LW depends much on *n*; for instance, for **DAD4**, LW is already dominant after 3 ns, while for **DAD6** the SW and LW emissions are seen with similar weights. At this delay time, LW is seen in **DAD8** and **DAD10** only as a small shoulder. Therefore, longer delay times are required to observe the LW features for these triads, as shown in Figure 3 for 20 ns. The appearance of the LW emission is particularly visible in the logarithmic TRES plots normalized at each wavelength (Figure 3, right-hand side), clearly showing the spectral drift from the SW to the LW emission over time for all triads, including $n = 8$, 10. The LW lifetime increases somewhat with the detection wavelength, which may hint at distributions of exciplex geometries

The overall photokinetics of inter- or intramolecular exciplexes are generally complex, and may largely differ depending on the exact composition of the system.[29,35] In fact, for the present **DAD*n*** triads, after generation of A^*, the two competitive deactivation pathways to fluorescence, i.e., quenching by eT_A and exciplex formation, cannot be described as simple competitive reactions with a constant radiative lifetime of [D···A^*], as in this case a strict correlation of τ_{SW} and $\Phi_{F,SW}$ would be expected, in disagreement with the current results, see Table 1. Therefore, the direct extraction of the attenuation factor β_{eT} from the fluorescence quenching rate as a function of spacer length[37,45,46] is not possible in the present case. Instead, the mismatch of τ_{PF} and $\Phi_{F,SW}$, together with the concurrent appearance of a delayed component in the SW band of **DAD4** evidences exciplex dissociation under regeneration of A^*,[29,35] see Scheme 1. The underlying reaction kinetics,[29] which were described in early publications,[47,48] formally correspond to those used to analyze other thermally activated processes like excited state proton transfer[47] or TADF.[49,50] Additionally, the mentioned mismatch of the exciplex rise time and the decay time of the SW emission evidences an intermediate (pre-associated) species in the creation of the exciplex, noted as [DA^*], i.e., where the excitation is still localized on A, see Scheme 1;[35] from here the charge transfer state [$D^{\bullet+}A^{\bullet-}$] is formed (k_{CTF}), which gives rise to the excimer emission. Furthermore, all rates are expected to vary among the different triads, in particular as a range of different triad conformations has to be anticipated. In fact, even the radiative deactivation from [D···A^*] is not expected to be constant for the various triads as the presence of the D moieties may impact the non-planarity of A; this, in turn, impacts the oscillator strength of the LE state, and with this the radiative rate. This is indeed observed in the quantum chemical calculations, which will be discussed hereafter. Moreover, also the formed exciplexes may adapt different conformations, including the formation with only one or two D moieties (D:A versus D:A:D). Therefore, the complexity of the photokinetics with a large number of rates and their variances impedes a precise rate constant analysis of the current system. Nevertheless, the lifetime data (τ_{P-}, τ_{DF}) and quantum yields (Φ_F, Φ_{SW}, Φ_{LW}) of the triads in $CHCl_3$ (Table 1) can be quite reasonably fitted by the above-mentioned reaction kinetics for a consecutive-competitive reaction with a reversible step,[47,48] allowing to

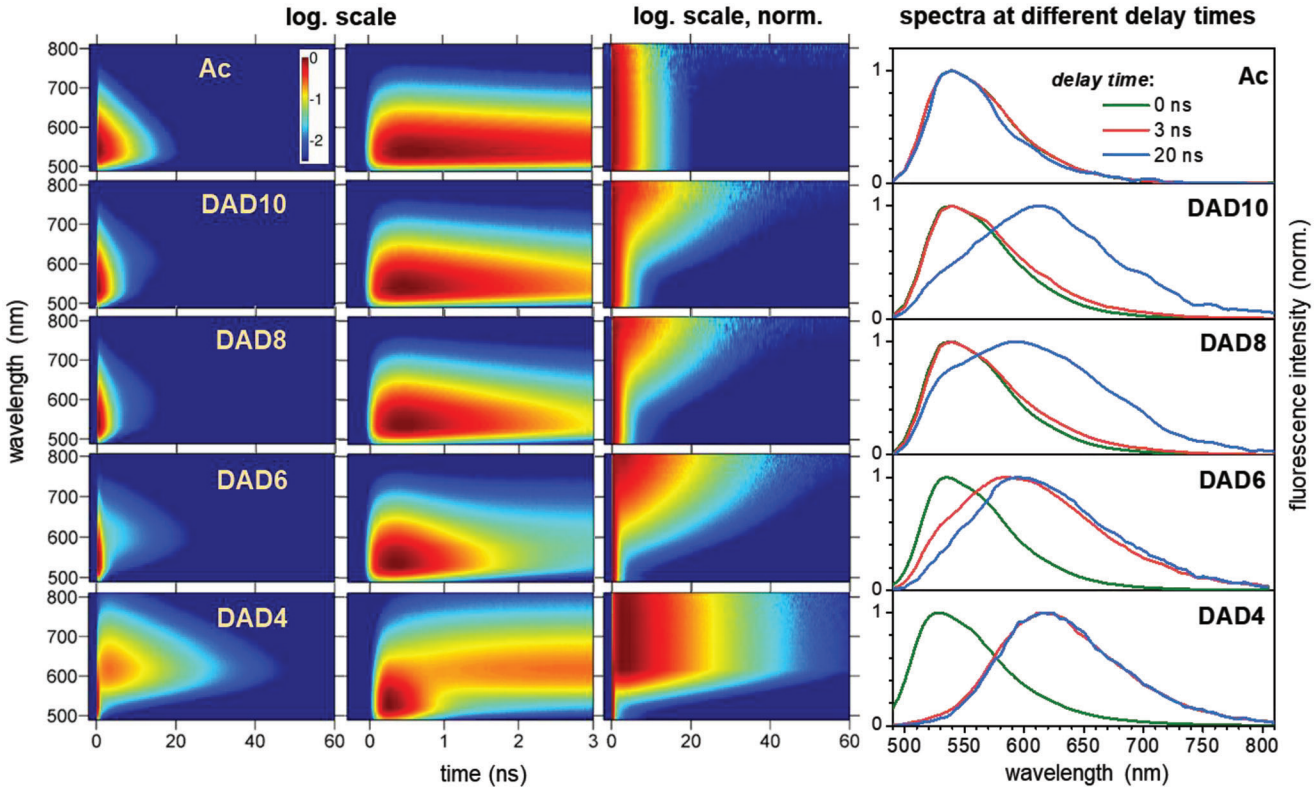

Figure 3. Time-resolved emission spectra (TRES) for the compounds under study in $CHCl_3$, normalized to the overall maximum and on a logarithmic scale, zoom of the latter into the time range up to 3 ns, and normalized at each wavelength, on a logarithmic scale (columns from left to right); right: spectra at different delay times. The color scale applies to all the subfigures.

extract at least the order of magnitude for the processes, as given in Scheme 1. Accordingly, the excited state lifetimes of [D···A*] and [D•+A•−] are fairly constant for the triads with $\tau_A^{-1} \approx 3 \times 10^8$ s^{-1} and $\tau_{ex}^{-1} \approx 1 \times 10^8$ s^{-1} (however with somewhat varying rates for k_r, k_{nr}). The rate constant of quenching by eT increases from $k_{eT,A} \approx 1 \times 10^7$ s^{-1} for **DAD10** to ≈1×10^8 s^{-1} for **DAD4** due to the shortened D··A separation, while the energy of the radical ion pair stays fairly constant according to the TD-DFT calculations (vide infra). Radical ion pair formation is however only a minor deactivation pathway in comparison with exciplex formation [DA*]. The latter increases from $k_a \approx 4 \times 10^8$ s^{-1} for **DAD10** (corresponding to an association time of $t_a = 2.5$ ns, see **Table 2**) to ≈4×10^9 s^{-1} for **DAD4** ($t_a = 0.25$ ns), due to the longer D–A separation (vide infra); on the other hand, the back reaction, i.e., excimer dissociation, increases only from $k_d \approx 1 \times 10^7$ s^{-1} to ≈3×10^7 s^{-1}. The data essentially explain the experimental observations (Table 1) with a strong shortening of the prompt lifetime τ_{PF} with decreasing spacer length, along with a more efficient formation of the emissive exciplex [D•+A•−]. The latter is formed from [DA*] with a rate constant $k_{CTF} = 6.7 \times 10^8$ s^{-1}; such two-step formation is in line with early suggestions by Weller.[35]

Table 2. Exciplex association times (t_a) for **DAD4** and **DAD10** in $CHCl_3$ as determined from the experiment (exp), from a free diffusion model (3D), quasi-1D diffusion, and the results from MD simulations.

	DAD4	DAD10
$t_{a,exp}$	0.25 ns	2.5 ns
$t_{a,3D}$	0.18 ns	0.46 ns
$t_{a,1D}$	0.55 ns	1.4 ns
$t_{a,MD}$	≈0.2 ns	≈1 ns

In order to rationalize the extracted rate constant k_a for association, the rate is first estimated within a simple diffusion model, based on diffusion of free carbazole (Cz), bridging the distance between the extended and stacked form; the latter can be estimated from the DFT calculations (vide infra) as the shortest distance d_{min} to ≈1.2 nm for **DAD4** and 1.9 nm for **DAD10**. The diffusion coefficient D of Cz is known in water and acetonitrile.[51,52] from which D in $CHCl_3$ can be interpolated by the Stokes–Einstein relation; using the viscosities of the solvents, this gives $D \approx 1.3 \times 10^{-5}$ cm^2 s^{-1}. Our MD simulations for free carbazole in $CHCl_3$ gave a very similar value with $D = 1.1 \pm 0.3 \times 10^{-5}$ cm^2 s^{-1}, as obtained via the mean square displacement; see Table S4 in the Supporting Information. The minimum diffusion time is then calculated from $t_{min} = d_{min}^2/(2xD)$ with $x = 1, 2, 3$ as the dimension of the diffusion. Calculating a reference value for free (3D) diffusion of Cz, one gets 0.18 ns for **DAD4** and 0.46 ns for **DAD10**, see Table 2. On the other side, assuming a quasi-1D trajectory due to the presence of the spacer, 0.55 ns for **DAD4** and 1.4 ns for **DAD10** is obtained. The results show indeed the same order of magnitude as the extracted association times reported above; nevertheless, the strong effect of spacer length, found in

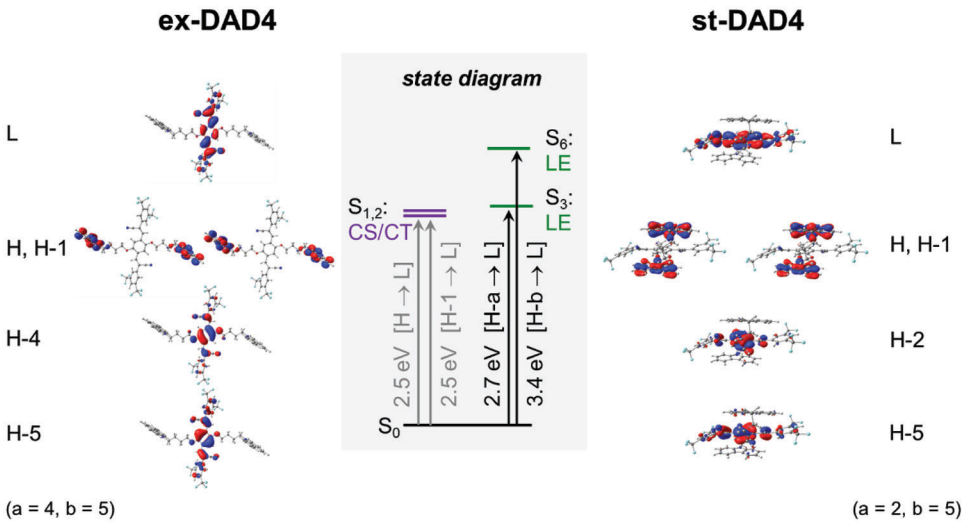

Figure 4. Simplified state diagram for the extended (**ex**) and stacked (**st**) forms of **DAD4**, displaying relevant electronic transitions, with the main contributions of the mono-electronic excitations ($S_{1,2}$: ≥98%; S_3: ≥97%; S_6: ≥85%) and the corresponding MO topologies (H = HOMO, L = LUMO). The energy difference between the two CS/CT states (S_1, S_2) is <0.05 eV; the two LE transitions ($S_{3,6}$) are mainly described by H-a→L and H-b→L, where $a = 4$, $b = 5$ for the **ex**-form, and $a = 2$, $b = 5$ for the **st**-form. Geometries optimized with the ωB97XD functional, electronic states calculated with the PBE0 functional.

the experiment, is not predicted in the simple diffusion model. In order to gain atomistic insight into the association process, we performed MD simulations of the triads in $CHCl_3$, giving a time constant t_a of ≈0.2 ns for **DAD4** and ≈1 ns for **DAD10** (Table 2), in reasonable agreement with the experimental values given above. It is noted that the difference between free 3D diffusion for **DAD4** is very similar to the restrained diffusion; this is ascribed to small variations in energy by the torsional adjustments of the spacer configurations.

2.2. Quantum-Chemical Treatment

In order to gain further insight into the geometry, electronic structure, and optical excitations of the triads, (TD-)DFT calculations were performed, using the Gaussian16 program package.[53] Geometry optimizations were carried out for two conformations: (i) fully extended (**ex**; imposing C_2 symmetry) and (ii) stacked form (**st**; C_i), to model the two extremes for D–A interactions, see **Figure 4**. As in particular the proper description of the stacked form requires the inclusion of dispersion, the ωB97XD functional was used for the DFT part. At this level of theory, the **st**-form is predicted to be more stable than the **ex**-form by ca. 1.5 eV (corresponding to a binding constant $\log K_a \approx 10$; somewhat varying on n), see Table S1 in the Supporting Information. In any case, it should be kept in mind that the very substantial energy difference between the two extreme cases does not necessarily reflect the dynamic situation in solution at room temperature. In the **st**-form, the two D moieties are forming a π-stacked DAD sandwich structure with A; however, the exact positioning depends sensitively on n. In fact, for **st-DAD4**, the D moieties are located asymmetrically on top and bottom of the central β-cyano-styryl moiety of A (see Figure 4); on the other hand, for longer spacers, the D moieties are located on top/bottom of the outer α-cyano-styryl moieties of A (see Figure S1, Supporting Information). For this reason, the acceptor unit is significantly more twisted for $n = 4$ in comparison with $n > 4$, see Table S1 in the Supporting Information.

The correct TD-DFT treatment of excited states with (partial) CT character is a matter of ongoing discussions; in fact, it was shown that for states with only partial CT character (i.e., with considerable non-zero oscillator strength f_{CT}), standard DFT functionals like B3LYP or PBE0 tend to fail,[54] due to the over-delocalization of the constituting wavefunctions. On the other hand, for states with very pronounced CT character (i.e., where the HOMO is localized in D and the LUMO in A, and, subsequently $f_{CT} \approx 0$), as in twisted D–A polyads or D–σ–A–σ–D triads, these functionals were shown to operate well.[11,14,18,55] As the current triads fall in this category, we utilized here the PBE0 functional for the TD part (in implicit solvent, $CHCl_3$, using the polarizable continuum model, PCM). This indeed reproduces the experimentally observed spectral features much better than, e.g., ωB97XD, M06-2X or CAM-B3LYP; in fact, the latter functionals predict the locally excited (LE) state as the lowest excited state (see Table S2, Supporting Information), in apparent disagreement with experiment. Within the PBE0 treatment, the overall description of the spectra is similar for the different spacer lengths n, and for both **st** and **ex** conformations, see Table S3 in the Supporting Information. The two intense bands in the experimental absorption spectrum (vide supra) are assigned to A-centered LE states; for instance, in **ex-DAD4** they correspond to S_3 and S_6 with 2.7 eV and 3.4 eV, and with similar oscillator strength ($f_3 = 0.73$, $f_6 = 0.75$), in reasonable agreement with experiment, see Figure 1.[56] On the other hand, two low-lying excited states ($S_{1,2}$) are found to be of pronounced charge transfer character, located at ca. 2.5 eV with small oscillator strength ($f << 0.01$); for details see Table S2 in the Supporting Information. For the **st**-form, these states correspond to CT states, while in the **ex**-form they represent CS states (i.e., the radical ion pair), which cannot be directly photoexcited from S_0 due to the large D···A separation.[57]

Table 3. Fluorescence quantum yields Φ_F and prompt (intensity-averaged) lifetimes τ_{PF} of **Ac**, **DAD4,** and **DAD10** in different solvents (MeOH = methanol), with respective viscosities (mPa s, at 25 °C)[60] and polarities (given in normalized $E_T(30)$ values, E_T^N).[58]

		n-Octane	Toluene	$CHCl_3$	MeOH
Viscosity	η	0.508	0.560	0.537	0.544
Polarity	E_T^N	0.012	0.099	0.259	0.762
Ac	Φ_F	0.59	0.60	0.41	0.30
	τ_F [ns]	4.47	4.55	3.39	3.35
DAD10	Φ_F	0.48	0.33	0.30	0.02
	τ_{PF} [ns]	1.73	1.36	1.39	0.47
DAD4	Φ_F	0.33	0.22	0.16	0.06
	τ_{PF} [ns]	1.48	0.36	0.21	0.73

For the **ex**-form, a small increase of the LE state energy (S_3) is observed with increasing *n*; at the same time, f_3 decreases somewhat. As the state description (almost exclusively HOMO-4→LUMO; see Table S2, Supporting Information) is the same for all *n*, the differences are ascribed to the topology of the MOs (Figure S3, Supporting Information), arising from (rather small) differences in the torsional angles within the vinylene units (Table S1, Supporting Information). This indicates that the presence of the D unit has a certain impact on the structure of A due to sterical demands; in any case, the differences in the calculations are somewhat more pronounced than in experiment. The changes in the CS state ($S_{1,2}$) energy are more pronounced; in fact, for $n = 10$, the CS states are found somewhat above the LE state.

In the stacked forms (**st-DAD*n***), the electronic situation is not very different from **ex-DAD*n***; in any case, the variations in energy are less pronounced. Remarkably, the oscillator strength of the LE-type $S_{3,6}$ states for $n = 4$, 6 are much smaller in the **st**-form compared to **ex** (e.g., $f_3 = 0.36$ for **st-DAD4**) due to reduced LCAO coefficients in the outer rings because of conformational constraints (Figure 4). Different from the **ex**-form, because of the close D–A separation in the **st**-form, the CT state can now be effectively populated after photoexcitation of A. The combined oscillator strength of the two low-lying CT states is calculated to be small (e.g., $f_{1+2} = 0.0033$ for **st-DAD4,** see Table S3 in the Supporting Information. This qualitatively rationalizes the long lifetime of the exciplex found experimentally (≈9.9 ns); however, a more quantitative treatment may require the inclusion of Herzberg–Teller coupling.

2.3. Solvent Effects on Fluorescence Quantum Yields and Lifetimes

The proposed dynamic nature of the exciplex formation in the current system should manifest itself in a pronounced dependency on environmental parameters, that is polarity and viscosity of the solvent, as well as temperature variation.

Polarity: To investigate the polarity effect, experiments were carried out in various solvents of similar viscosity, but varying polarity (**Table 3**), i.e., *n*-octane, toluene, $CHCl_3$, and methanol (MeOH). It is emphasized that the analysis is complicated by the fact that also the SW emission (i.e., from A^*) is polarity dependent. In fact, also the emission of the acceptor alone, **Ac**, shows a systematic bathochromic shift with increasing polarity, i.e., from 515 nm in *n*-octane to 548 nm in MeOH (**Figure 5**). At the same time, the structured band shape in nonpolar *n*-octane evolves towards unstructured features in polar solvents, seconded by a systematic decrease of Φ_F from 0.6 in *n*-octane to 0.3 in MeOH; see Table 3. The decrease of (intensity-averaged) τ_F is less pronounced, while the decay is less exponential at higher polarity. All effects are attributed to a small but non-negligible partial CT character of the LE ($S_0 \leftrightarrow S_1$) transition in **Ac** (see Figure S3, Supporting Information). This gives rise to a reorganization of the polar solvent shell after photoexcitation.[58] In turn, the **Ac** structure in S_1 suffers from stronger reorganization with increasing polarity, which decreases $k_r = \Phi_F/\tau_F$. The geometry change also rationalizes the observed non-exponential fluorescence decay of **Ac**; details of this study will be given in a forthcoming paper.

Using the spectral positions of the **Ac** emission as references for SW emission of the triads, we can assign the spectrum of **DAD4** in MeOH (556 nm) mainly to SW emission; at the same time, the emission is effectively quenched (with $\Phi_F = 0.02$; see Table 3), due to the stabilization of the radical ion pair.[59] In any case, the spectrum is somewhat broadened in the low energy part in comparison with **Ac**, pointing to the presence of the exciplex, but to a very minor degree. This is consistent with the time traces, recorded in the LW region (i.e., at 680 nm), which shows a long, but weak component of ≈7.6 ns, see Figure S10 and Table S6 in the Supporting Information. This evidences the dominance of quenching by eT in polar solvents in line with former studies.[35] In stark contrast, for lower polarity, the SW emission is seen only as a shoulder, so that the emission is dominated by the LW band; at the same time, a strong hypsochromic shift of λ_{LW} from 613 nm in toluene and $CHCl_3$ to 584 nm in *n*-octane is observed (with a spectral fraction of $x_{LW} = 80\%$, as determined by spectral decomposition, see Figure S9, Supporting Information) In all, the results demonstrate only a small polarity effect in exciplex formation, but a significant effect on the quenching pathway.

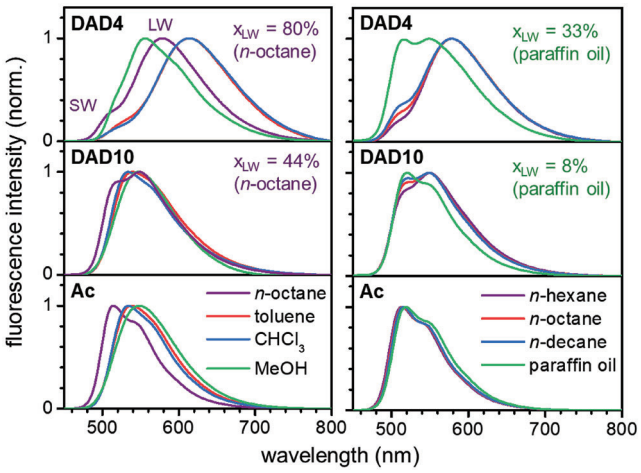

Figure 5. Fluorescence spectra of **Ac**, **DAD10**, and **DAD4** in solvents of different polarity (left) and viscosity (right); fractional intensities of the long wavelength emission x_{LW} were obtained by spectral decomposition, see Figure S9 in the Supporting Information.

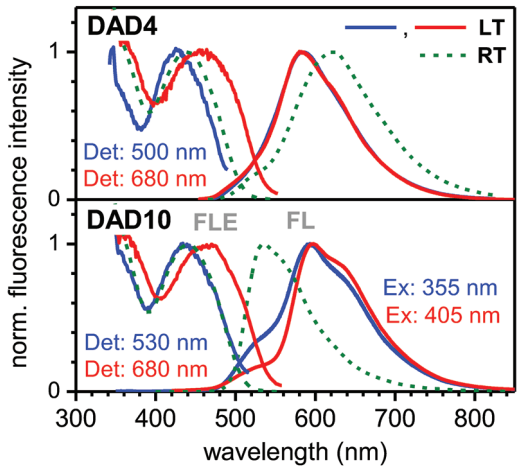

Figure 6. Fluorescence emission (FL, right) and excitation (FLE; left) spectra of **DAD4** (top) and **DAD10** (bottom) in $CHCl_3$ ($c = 1 \times 10^{-5}$ M) at low temperature (LT; FL at 65 K, FLE at 77 K: blue and red solid lines) under different excitation (detection) conditions for FL (FLE), $\lambda_{ex} = 355$ nm (blue), 405 nm (red), and $\lambda_{det} = 500/530$ nm (blue), 680 nm (red). FL and FLE spectra at room temperature (RT, green dashed lines, $\lambda_{ex} = 405$ nm) are shown for comparison.

Viscosity: To investigate the viscosity effect, **DAD4** (i.e., the triad with the highest tendency for exciplex formation) was dissolved in saturated hydrocarbons at ambient conditions with increasing viscosity, i.e., *n*-hexane ($\eta = 0.300$ mPa s), *n*-octane (0.508 mPa s), *n*-decane (0.838 mPa s),[60] and paraffin oil (ca. 100 mPa s), see Figure 5. At low viscosities, a small increase of the SW intensity with η is observed, while the overall emission is dominated by the LW band. In paraffin oil, the LW band significantly decreases, and the spectrum is now dominated by the SW emission ($x_{SW} =$ 67%; as determined by spectral decomposition, see Figure S9, Supporting Information). This indeed proves that the dynamic exciplex formation is effectively suppressed in highly viscous media, as expected. Concomitantly, for **DAD10**, the LW intensity reduces from 44% in *n*-hexane (low viscosity, low polarity) to 8% in paraffin oil, see Figure 5 and Figures S9, S15 in the Supporting Information. In order to gain further insight into the dynamic exciplex formation, we repeated the MD simulations for **DAD4** in paraffin oil. Indeed, the collapse of the extended to the stacked conformation is now extended to several nanoseconds, compared to ≈0.2 ns in $CHCl_3$. Finally, due to the dynamic nature of exciplex formation, the process is completely inhibited in solid solutions, by embedding **DAD4** at low concentrations in poly(methyl methacrylate; PMMA); in fact, only SW emission is observed in this case, see Figure S17 in the Supporting Information.

Temperature. The low temperature (LT) behavior of **DAD4** and **DAD10** in $CHCl_3$ at $T = 65$ K was investigated at different concentrations, see **Figure 6** and Figure S13 in the Supporting Information. For **DAD4** at $c = 1 \times 10^{-5}$ M, the emission spectrum shows a similar shape in comparison to room temperature (RT), dominated by the LW band, but being hypsochromically shifted by 0.13 eV vs RT, see Figure 6. The SW band, obtained by spectral decomposition, on the other hand, shows a small bathochromic shift. Importantly, the fluorescence excitation (FLE) spectrum shows a significant dependence on the detection wavelength λ_{det}; for detection at λ_{SW} (500 nm), the spectrum is very similar to the FLE spectrum at RT, while under λ_{LW} detection (680 nm), the FLE spectrum exhibits a significant bathochromic shift. This is in stark contrast to the FLE at RT, which does not show a dependency on λ_{det} (vide supra), evidencing a fundamentally different scenario at RT and LT, that is dynamic exciplex formation in the liquid, but formation of static (i.e., ground-state) CT complexes in the frozen solution. The formation of the CT complex is already observed at $c = 1 \times 10^{-6}$ M (Figure S13, Supporting Information), evidencing an intramolecular scenario. On the other hand, a significant concentration dependence of the spectral features is observed (Figure S13, Supporting Information), so that at concentrations of 10^{-4} M and higher only LW emission is observed. This suggests the concomitant generation of intermolecular static CT complexes at higher concentrations. As discussed above, the exciplex at RT is formed in a dynamic manner from the **ex**-form, while the LT conditions evidently freeze out the **st**-form in the ground state, as well as intermolecular CT complexes. The CT complex is stabilized by 0.17 eV versus the **ex**-form, as extracted from the bathochromic shift of the FLE spectrum. The TD-DFT calculated bathochromic shift is significantly smaller (0.03 eV, see Table S3, Supporting Information), which may in part be related with the shortcomings of the linear response PCM used in this work. On the other side, also mutual polarization of the D and A moieties in the **st**-conformation will contribute to the bathochromic shift,[10] which might be insufficiently described in the TD-DFT scheme. Such polarization, however, cannot be the source of the LW band shift upon cooling, as the LW band shows the opposite behavior, i.e., a hypsochromic shift. We thus rather infer that the latter originates from somewhat different intra- and/or intermolecular D–A arrangements, as the emission color should indeed sensitively depend on the exact mutual position of the moieties; this was in particular shown for excimers.[28,34,61]

Turning from **DAD4** to **DAD10**, the spectral changes in FL upon freezing are more drastic, as at RT conditions, dynamic exciplex formation in **DAD10** was unlikely to occur due to the long spacer (vide supra). The decrease in solubility at LT conditions promotes intramolecular stacking already in the electronic ground state, giving rise to a static CT complex; this is apparently highly effective, so that the FL is now dominated by the LW band, see Figure 6. In any case, the fraction of LW is still significantly smaller compared to **DAD4**, reflecting the lower probability for stacking due to the longer spacer in **DAD10**. Concomitantly, shifting the excitation wavelength towards the red, the probability of exciting the **st**-form increases, due to the presence of the low-lying CT state; this enhances the LW fraction in the FL spectrum (i.e., compare the blue and red spectra in Figure 6). As in **DAD4**, also **DAD10** shows a significant concentration dependence, evidencing the concomitant formation of intermolecular CT complexes. In all, the LT studies demonstrate how dynamic exciplex formation can be transformed to a static, intramolecular CT complex by spatial confinement, and how spectroscopy allows to monitor these changes.

2.4. Emission of the Molecular Solids

Importantly, the current study allows also for a more nuanced view on the solid-state properties of the triads (i.e., powders or

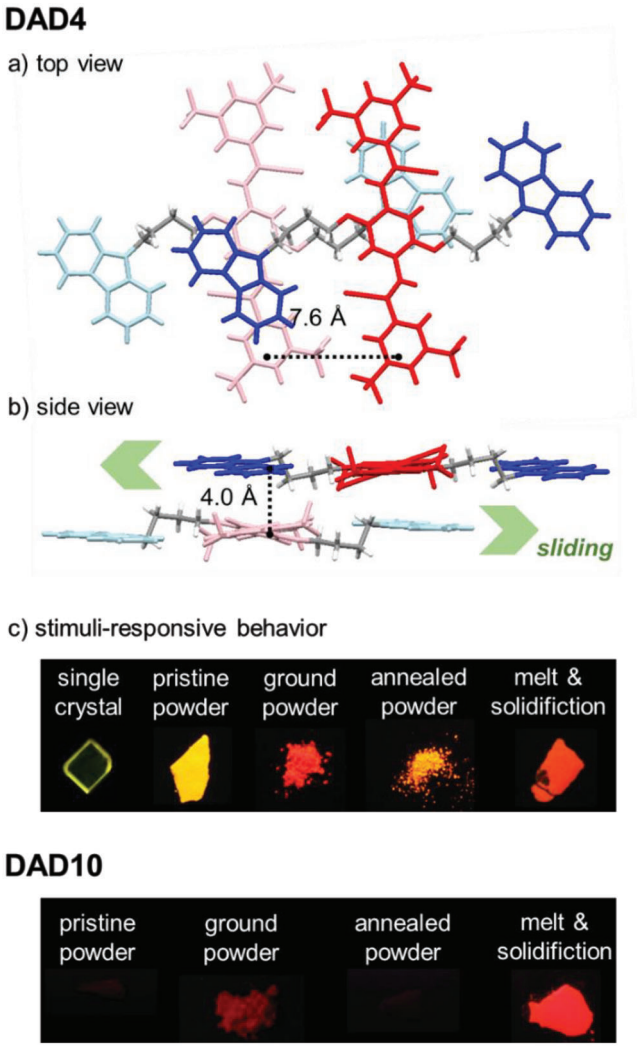

Figure 7. Solid-state properties of the molecular triads **DAD*n***. Top: nearest neighbor arrangement in **DAD4** crystals (CCDC 2 265 264) with D moieties in blue and A moieties in red; a) top view, b) side view, highlighting the sliding plane (green arrows); c) fluorescence images of the **DAD4** single crystal and the powder samples and their stimuli-responsive behavior. Bottom: fluorescence on/off switching for $n > 4$; here exemplified for **DAD10**.

films). In fact, all **DAD*n*** triads were reported to show stimuli-responsive luminescence behavior, when applying pressure or temperature. While for $n = 4$ yellow/red fluorescence color switching was observed, for $n > 4$ fluorescence on/off switching occurred between pristine or annealed powder ("off" state) and ground powder ("on" state),[15] see **Figure 7**. This was tentatively attributed back then to an intramolecular conformational change between the extended and the stacked form. Our current results, however, clearly evidence the emissive character of the CT complexes; in fact, the static CT complexes in frozen solution absorb and emit at the same spectral positions as the (pure) spin-cast films reported by Kwon et al.[15] We therefore ascribe the emissive properties of spin-cast films and ground powders of all triads to the presence of static CT complexes. On the other hand, we have demonstrated in the current work the subtle competition between the fluorescence of the CT complex and fluorescence quenching by eT, in particular for small distance between the D and A moieties. Therefore, in the solid state, the effectiveness of exciplex emission will sensitively depend on the exact geometric positioning of D and A. It is thus evident that even small perturbations in the intra- and/or intermolecular arrangement of the dyads in the solid state, as induced by external stimuli, may generate effective fluorescence on-off switching by subtle balancing of the CT emission versus quenching through unfavorable D–A positioning.

The exact mechanism of fluorescence switching is however difficult to prove without structural information. However, crystallization of the materials turned out to be challenging for $n > 4$; we ascribe these difficulties to the enlarged conformational space with longer spacer length, which flattens the potential energy surface for intra- and intermolecular interactions. Fortunately, the growth of **DAD4** single crystals could be achieved (see SI for details), whereas single crystal growth failed for the other triads. The **DAD4** crystals fluoresces yellow under UV irradiation, very similar to the pristine powder sample, see Figure 7 and Figure S17 in the Supporting Information. Upon grinding the pristine powder, the color turns red, and turns back to yellow upon annealing at 120 °C. Here, the red color corresponds to that of the exciplex in solution, see Figure S17 in the Supporting Information. In fact, this behavior remained an open question in ref. [15] which can now, however, be answered in light of the current results. In the **DAD4** crystal, the molecules adapt an extended conformation with a significantly twisted backbone of the acceptor unit (see Figure 7 and the SI for further details); in any case, it is less twisted than what was calculated for the free molecule, demonstrating the "twist elasticity" of the DCS motif.[62] The triads are slipped along the short (x) axis of DCS by ≈7.6 Å, so that pronounced exciton formation between the DCS units can be neglected.[10] Instead, the Cz (D) moieties are located above the vinylene unit of the DCS core (A) with a mean distance of 4.0 Å (see Figure S21 in the Supporting Information for details), providing sufficient π-overlap to form a D–A CT complex between the adjacent triads. The molecules form sliding planes (see Figure 7), which rationalizes the facile response to external stimuli. Hence, upon grinding, the relative position of D and A of the adjacent triads will change their position. Plausible is a positioning of Cz on the central ring of the adjacent DCS core, thus generating the same electronic situation which was predicted for the exciplex in an intramolecular fashion, but here in an intermolecular manner. It should be noted in this context that also powder samples of the acceptor alone (**Ac**) emit red, see Figure S19 in the Supporting Information. Therefore, it cannot be excluded that the red color of the **DAD4** ground powder may originate from DCS stacks generated through an x-slip of the molecules upon mechanical stimuli.

For the longer spacers, no structural data are available, as all attempts to grow the corresponding crystal did not succeed. In any case, it is evident from the negligible emission in the pristine powder (as well as after thermal annealing) that the thermodynamically stable mutual arrangement of the D and A moieties in this case do not provide sufficient π-overlap to allow for an emissive CT state, but quenches fluorescence through unfavorable D:A positioning. Mechanical force then displaces the molecules along the sliding axis, which allows for sufficient π-overlap

to generate red emission, see bottom of Figure 7. In all, the current findings provide an important complement to the work by Kwon et al.;[15] the current results may inspire further investigations in stimuli-responsive materials relying on the subtle interplay of complex photophysical deactivation pathways. Moreover, this work may be relevant in the fundamental understanding for the occurrence of emissive exciplexes in OLEDs[6] or reconsideration of organic exciplex lasers.[63]

3. Conclusions

A holistic picture on the complex photophysical pathways of D–σ–A–σ–D triads with varying flexible spacer lengths (n = 4–10 carbon atoms) was established in liquid and solid solution by combining (steady-state and time-resolved) optical spectroscopy with TD-DFT and MD computational studies. In liquid solution, the competitive dynamic CT state formation with subsequent exciplex emission versus (minor) quenching by electron transfer (eT) via a radical ion pair has been quantified, identifying an optimized system with 14% exciplex fluorescence quantum yield. In solid solution, a fluorescent static CT complex is formed upon freezing/solidification; this is assigned also as the fluorescent phase in the film samples. Thermal stimulus of the film (annealing) either: i) breaks the CT complex, leading to on/off fluorescence switching by effective fluorescence quenching (for $n >$ 4), or ii) modulates the geometry of the CT complex, which results in a change of the emission color ($n = 4$). In all, the study emphasizes the imperative for a holistic, detailed understanding of compounds with complex photophysics, as achieved here, in order to reach the ultimate goal of targeted design of novel materials in exciplex-based applications in sensing, OLEDs or lasing.

Supporting Information

Supporting Information is available from the Wiley Online Library or from the author.

Acknowledgements

B.M.-M. and J.G. acknowledge funding by the Spanish Ministerio de Economía y Competitividad/Ministerio de Ciencia e Innovación (MINECO/MICIN-FEDER projects CTQ2017-87054, PID2022-138222NB-C21, PID2022-138222NB-C22). R.W. acknowledges funding from MICIN-FEDER projects RTI2018-097508-B-I00, PID2021-128313OB-I00 and TED2021-131018B-C22 and from the Comunidad de Madrid and the European Union structural funds through grant S2018/NMT-4511. The work in Madrid was further supported by the Severo Ochoa program for Centers of Excellence in R&D of the MICIN (CEX2020-001039-S) and by the Campus of International Excellence (CEI) UAM+CSIC. S.F. acknowledges a grant from the China Scholarship Council (CSC; grant no. 202008330343). M.S.K. acknowledges support from the National Research Foundation of Korea (NRF) funded by the Korean government (MSIT; grant no. 2022R1A2C2011627 and 2021R1A5A1030054).

Conflict of Interest

The authors declare no conflict of interest.

Data Availability Statement

The data that support the findings of this study are available from the corresponding author upon reasonable request.

Keywords

exciplexes, fluorescence, photophysics, organic optoelectronics, stimuli-responsive materials

Received: July 8, 2023
Revised: August 24, 2023
Published online:

[1] Z. Wu, J. Nitsch, T. B. Marder, *Adv. Opt. Mater.* **2021**, *9*, 2100411.
[2] M. Y. Wong, E. Zysman-Colman, *Adv. Mater.* **2017**, *29*, 1605444.
[3] T. Itoh, *Chem. Rev.* **2012**, *112*, 4541.
[4] S. K. Behera, S. Y. Park, J. Gierschner, *Angew. Chem., Int. Ed.* **2021**, *60*, 22624.
[5] N. A. Kukhta, M. R. Bryce, *Mater. Horiz.* **2021**, *8*, 33.
[6] a) M. Sarma, K.-T. Wong, *ACS Appl. Mater. Interfaces* **2018**, *10*, 19279; b) M. Zhang, C.-J. Zheng, H. Lin, S.-L. Tao, *Mater. Horiz.* **2021**, *8*, 401; c) J. Gu, Z. Tang, H. Guo, Y. Chen, J. Xiao, Z. Chen, L. Xiao, *J. Mater. Chem. C* **2022**,*10*, 4521.
[7] D. Beljonne, J. Cornil, L. Muccioli, C. Zannoni, J.-L. Brédas, F. Castet, *Chem. Mater.* **2011**, *23*, 591.
[8] a) M. Wykes, B. M. Medina, J. Gierschner, *Front. Chem.* **2013**, *1*, 35; b) A. D. Thilanga Liyanage, B. Milián-Medina, B. Zhang, J. Gierschner, M. D. Watson, *Macromol. Chem. Phys.* **2016**, *217*, 2068.
[9] a) J. Gierschner, M. Ehni, H.-J. Egelhaaf, B. Milián Medina, D. Beljonne, H. Benmansour, G. C. Bazan, *J. Chem. Phys.* **2005**, *123*, 144914; b) S. Oh, S. K. Park, B. H. Jhun, J. C. Roldao, J. H. Kim, M.-W. Choi, C. H. Ryoo, S. Jung, N. Demitri, R. Fischer, I. E. Serdiuk, R. Resel, J. Gierschner, S. Y. Park, *J. Phys. Chem. C* **2020**, *37*, 20377.
[10] J. Gierschner, J. Shi, D. Roca-Sanjuán, B. Milián-Medina, S. Varghese, S. Y. Park, *Adv. Opt. Mater.* **2021**, *9*, 2002251.
[11] Y. Olivier, J. C. Sancho-García, L. Muccioli, G. D'Avino, D. Beljonne, *J. Phys. Chem. Lett.* **2018**, *9*, 6149.
[12] S. Ramírez-Barroso, F. Romeo-Gella, J. M. Fernández-García, S. Feng, L. Martínez-Fernández, D. García-Fresnadillo, I. Corral, N. Martín, R. Wannemacher, *Adv. Mater.* **2023**, *35*, 2212064.
[13] M. A. Bryden, E. Zysman-Colman, *Chem. Soc. Rev.* **2021**, *50*, 7587.
[14] V. K. Singh, C. Yu, S. Badgujar, Y. Kim, Y. Kwon, D. Kim, J. Lee, T. Akhter, G. Thangavel, L. S. Park, J. Lee, P. C. Nandajan, R. Wannemacher, B. Milián-Medina, L. Lüer, K. S. Kim, J. Gierschner, M. S. Kwon, *Nat. Catal.* **2018**, *1*, 794.
[15] M. S. Kwon, J. Gierschner, S.-J. Yoon, S. Y. Park, *Adv. Mater.* **2012**, *24*, 5487.
[16] M. S. Kwon, J. Gierschner, J. Seo, S. Y. Park, *J. Mater. Chem. C* **2014**, *2*, 2552.
[17] S. Thazhathethil, T. Muramatsu, N. Tamaoki, C. Weder, Y. Sagara, *Angew. Chem., Int. Ed.* **2022**, *61*, e202209225.
[18] B. Milián-Medina, J. Gierschner, *Org. Electron.* **2012**, *13*, 985.
[19] T. Hatakeyama, K. Shiren, K. Nakajima, S. Nomura, S. Nakatsuka, K. Kinoshita, J. Ni, Y. Ono, T. Ikuta, *Adv. Mater.* **2016**, *28*, 2777.
[20] H. Meier, *Angew. Chem., Int. Ed.* **2005**, *44*, 2482.
[21] a) Y.-J. Cho, A.-R. Lee, S.-Y. Kim, M. Cho, W.-S. Han, H.-J. Son, D. W. Cho, S. O. Kang, *Phys. Chem. Chem. Phys.* **2016**, *18*, 22921; b) M. Bayda-Smykaj, G. Burdzinski, M. Ludwiczak, G. L. Hug, B. Marciniak, *J. Phys. Chem. C* **2020**, *124*, 19522; c) M.-J. Kim, M. Ahn, M. Chae, S. Kim, D. Kim, K.-R. Wee, *RSC. Adv.* **2021**, *11*, 34945.
[22] S. J. Strickler, R. A. Berg, *J. Chem. Phys.* **1962**, *37*, 814.
[23] T. Dutta, K. B. Woody, S. R. Parkin, M. D. Watson, J. Gierschner, *J. Am. Chem. Soc.* **2009**, *131*, 17321.
[24] a) S.-Y. Kim, Y.-J. Cho, A.-R. Lee, H. Son, W.-S. Han, D. W. Cho, S. O. Kang, *Phys. Chem. Chem. Phys.* **2017**, *19*, 426; b) M.-J. Kim, M. Ahn, J. H. Shim, K.-R. Wee, *Phys. Chem. Chem. Phys.* **2020**, *22*, 3370.

[25] Z. R. Grabowski, K. Rotkiewicz, W. Rettig, *Chem. Rev.* **2003**, *103*, 3899.
[26] a) J. B. Birks, *Nature* **1967**, *214*, 1187; b) G. J. Kavarnos, N. J. Turro, *Chem. Rev.* **1986**, *86*, 401.
[27] T. Förster, *Excimers and Exciplexes*, in (Eds: M. Gordon, W. R. Ware), Elsevier, New York **1975**.
[28] F. M. Winnik, *Chem. Rev.* **1993**, *93*, 587.
[29] P. Vanderauwera, F. C. DeSchryver, A. Weller, M. A. Winnik, K. A. Zachariasse, *J. Phys. Chem.* **1984**, *88*, 2964.
[30] H.-G. Busmann, H. Staerk, A. Weller, *J. Chem. Phys.* **1989**, *91*, 4098.
[31] a) H. Staerk, W. Kühnle, A. Weller, U. Werner, *Z. Phys. Chem.* **1995**, *188*, 61; b) A. Zehnacker, F. Lahmani, J. P. Desvergne, H. Bouas-Laurent, *Chem. Phys. Lett.* **1998**, *293*, 357; c) J. Kawakami, J. Nakamura, M. Iwamura, *J. Photochem. Photobiol. A: Chem.* **2001**, *140*, 199; d) F. Galindo, M. I. Burguete, S. V. Luis, *Chem. Phys.* **2004**, *302*, 287; e) H. Lemmetyinen, N. V. Tkachenko, A. Efimov, M. Niemi, *J. Phys. Chem. C* **2009**, *113*, 11475.
[32] F. D. Lewis, J. M. Wagner-Brennan, J. M. Denari, *J. Phys. Chem. A* **1998**, *102*, 519.
[33] M. Martínez-Abadía, S. Varghese, P. Romero, J. Gierschner, R. Giménez, M. B. Ros, *Adv. Opt. Mater.* **2017**, *5*, 1600860.
[34] F. Hirayama, *J. Chem. Phys.* **1965**, *42*, 3163.
[35] A. Weller, *Pure Appl. Chem.* **1982**, *54*,1885.
[36] Y. Hou, X. Zhang, K. Chen, D. Liu, Z. Wang, Q. Liu, J. Zhao, A. Barbon, *J. Mater. Chem. C* **2019**, *7*, 12048.
[37] M. Gilbert, B. Albinsson, *Chem. Soc. Rev.* **2015**, *44*, 845.
[38] M. Natali, S. Campagna, F. Scandola, *Chem. Soc. Rev.* **2014**, *43*, 4005.
[39] K. J. Lee, Y. Xiao, E. S. Kim, F. Mathevet, L. Mager, O. Cregut, F. Fages, J.-C. Ribierre, J. W. Wu, A. D'Aleó, *ACS Photonics* **2019**, *6*, 2649.
[40] J. Shi, L. E. Aguilar Suarez, S.-J. Yoon, S. Varghese, C. Serpa, S. Y. Park, L. Lüer, D. Roca-Sanjuán, B. Milián-Medina, J. Gierschner, *J. Phys. Chem. C* **2017**, *121*, 23166.
[41] J. Shi, L. M. Izquierdo, S. Oh, S. Y. Park, B. Milián-Medina, D. Roca-Sanjuán, J. Gierschner, *Org. Chem. Front.* **2019**, *6*, 1948.
[42] M. A. Izquierdo, J. Shi, S. Oh, S. Y. Park, B. Milián-Medina, J. Gierschner, D. Roca-Sanjuán, *Phys. Chem. Chem. Phys.* **2019**, *21*, 22429.
[43] D. Oelkrug, J. Gierschner, H.-J. Egelhaaf, L. Lüer, A. Tompert, K. Müllen, U. Stalmach, H. Meier, *Synth. Met.* **2001**, *121*, 1693.
[44] D. Oelkrug, A. Tompert, J. Gierschner, H.-J. Egelhaaf, M. Hanack, M. Hohloch, E. Steinhuber, *J. Phys. Chem. B* **1998**, *102*, 1902.
[45] M. R. Wasielewski, *Chem. Rev.* **1992**, *92*, 435.
[46] B. Albinsson, J. Mårtensson, *J. Photochem. Photobiol. C: Photochem. Rev.* **2008**, *9*, 138.
[47] A. Weller, *Z. Phys. Chem.* **1958**, *15*, 438.
[48] J. B. Birks, *Photophysics of Aromatic Molecules*, Wiley-Interscience, New York **1970**, Ch. 7.
[49] *Highly Efficient OLEDs: Materials Based on Thermally Activated Delayed Fluorescence* (Ed: H. Yersin), Wiley-VCH, Weinheim, Germany **2019**.
[50] In principle, [D···A*] can be also thermally repopulated from the CS state [D●+···A●-], which may however be ere neglected as BeT to the ground state is expected to be fast.
[51] Chemical Properties for Calculation of Impact to Ground Water Soil Remediation Standards, New Jersey Department of Environmental Protection, https://doi.org/10.7282/T3Z0385G.
[52] J. M. Ahn, T. S. Ratani, K. I. Hannoun, G. C. Fu, J. C. Peters, *J. Am. Chem. Soc.* **2017**, *139*, 12716.
[53] M. J. Frisch, G. W. Trucks, H. B. Schlegel, G. E. Scuseria, M. A. Robb, J. R. Cheeseman, G. Scalmani, V. Barone, G. A. Petersson, H. Nakatsuji, X. Li, M. Caricato, A. V. Marenich, J. Bloino, B. G. Janesko, R. Gomperts, B. Mennucci, H. P. Hratchian, J. V. Ortiz, A. F. Izmaylov, J. L. Sonnenberg, D. Williams-Young, F. Ding, F. Lipparini, F. Egidi, J. Goings, B. Peng, A. Petrone, T. Henderson, D. Ranasinghe, et al., Gaussian 16, Revision C.01, Gaussian, Inc., Wallingford, CT, USA, **2016**.
[54] A. Dreuw, M. Head-Gordon, *J. Am. Chem. Soc.* **2004**, *126*, 4007.
[55] N. Tang, J. Zhou, L. Wang, M. Stolte, G. Xie, X. Wen, L. Liu, F. Würthner, J. Gierschner, Z. Xie, *Nat. Commun.* **2023**, *14*, 1922.
[56] It is noted that the triads do not constitute a TADF system, even in the st-form, despite the strong CT character of $S_{1,2}$. In fact, while the exchange energy of $S_{1,2}$ with the correlated triplet is practically zero, these triplet states do not constitute the lowest triplet states. This is due to the fact that the LE state S_3 is energetically close-by; therefore, its correlated triplet LE state is found well below the triplet CT states, and the overall singlet-triplet gap ΔE_{ST} is relatively large (0.4–0.5 eV; see Table S3, Supporting Information), which inhibits effective TADF. It is unclear, to which degree the triplet manifold is populated. In any case, phosphorescence is practically non-existent, as our gated low-temperature measurements show; see Figure S11 in the Supporting Information.
[57] In fact, even for a nonbonded D–A pair with distance of 40 Å, TD-DFT still formally generates states with charge transfer character (although at somewhat higher energy) despite the large distance (see Figure S5, Supporting Information); for such large distances the CS nature of these states is self-evident.
[58] C. Reichardt, *Solvents and Solvent Effects in Organic Chemistry*, 3rd ed., Wiley-VCH, Weinheim, Germany, **2003**.
[59] D. Rehm, A. Weller, *Israel J. Chem.* **1970**, *8*, 259.
[60] *CRC Handbook of Chemistry and Physics*, 82nd ed., CRC Press, Boca Raton, FL, USA **2001**.
[61] S. Reiter, M. K. Roos, R. de Vivie-Riedle, *ChemPhotoChem* **2019**, *3*, 881.
[62] J. Shi, S.-J. Yoon, L. Viani, S. Y. Park, B. Milián-Medina, J. Gierschner, *Adv. Opt. Mater.* **2017**, *5*, 1700340.
[63] N. Nakashima, N. Mataga, C. Yamanaka, R. Ide, S. Misumi, *Chem. Phys. Lett.* **1973**, *18*, 386.